HHS Public Access

Author manuscript

Nat Struct Mol Biol. Author manuscript; available in PMC 2015 August 01.

Published in final edited form as:

Nat Struct Mol Biol. 2015 February ; 22(2): 132–137. doi:10.1038/nsmb.2953.

Ring closure activates yeast γTuRC for species-specific microtubule nucleation

Justin M. Kollman[1], **Charles H. Greenberg**[2,3,4], **Sam Li**[5], **Michelle Moritz**[5], **Alex Zelter**[1], **Kimberly K. Fong**[1], **Jose-Jesus Fernandez**[6], **Andrej Sali**[2,3,4], **John Kilmartin**[7], **Trisha N. Davis**[1], and **David A. Agard**[5,8,*]

[1]Department of Biochemistry, University of Washington, Seattle, WA, USA [2]Department of Bioengineering and Therapeutic Sciences, University of California at San Francisco, San Francisco, CA, USA [3]Department of Pharmaceutical Chemistry, University of California at San Francisco, San Francisco, CA, USA [4]California Institute for Quantitative Biosciences (QB3), University of California at San Francisco, San Francisco, CA, USA [5]Department of Biochemistry and Biophysics, University of California at San Francisco, San Francisco, CA, USA [6]Centro Nacional de Biotecnología, Consejo Superior de Investigaciones Cientificas, Madrid, Spain [7]Medical Research Council Laboratory of Molecular Biology, Cambridge, England [8]Howard Hughes Medical Institute, University of California at San Francisco, San Francisco, California, USA

Abstract

The γ-tubulin ring complex (γTuRC) is the primary microtubule nucleator in cells. γTuRC is assembled from repeating γ-tubulin small complex (γTuSC) subunits and is thought to function as a template by presenting a γ-tubulin ring that mimics microtubule geometry. However, a previous yeast γTuRC structure showed γTuSC in an open conformation that prevents matching to microtubule symmetry. By contrast, we show here that γ-tubulin complexes are in a closed conformation when attached to microtubules. To confirm its functional importance we trapped the closed state and determined its structure, showing that the γ-tubulin ring precisely matches microtubule symmetry and providing detailed insight into γTuRC architecture. Importantly, the closed state is a stronger nucleator, suggesting this conformational switch may allosterically

*Correspondence: David A. Agard, University of California at San Francisco, Mission Bay, Genentech Hall, 600 16th Street, Room S412D, San Francisco, CA 94158-2517, agard@msg.ucsf.edu.

DATA ACCESSION CODES

The structures of the capped microtubule end and γTuSC^{CC}–Spc110$^{1–220}$ filament have been deposited in the EM data bank (accession numbers EMD-5989 and EMD-2799, respectively).

AUTHOR CONTRIBUTIONS

J.M.K. prepared samples, collected cryo-EM data, performed three-dimensional reconstructions, analyzed data, and wrote the paper. C.H.G. performed molecular modeling, analyzed results, and contributed to writing the paper. S. L. prepared samples, collected tomographic data, performed tomographic reconstructions, and analyzed data. M.M. performed microtubule nucleation assays and analyzed data. A.Z. generated expression constructs and optimized protein expression. K.K.F. performed yeast viability assays and spindle morphology experiments and analyzed data. J.J.F. assisted with subvolume averaging. A.S. analyzed data and contributed to writing the paper. J.K. provided samples and analyzed data. T.N.D. analyzed data and contributed to writing the paper. D.A.A. analyzed data and contributed to writing the paper.

control γTuRC activity. Finally, we demonstrate that γTuRCs have a profound preference for tubulin from the same species.

Microtubule nucleation is mediated *in vivo* by γ-tubulin complexes, which allow cells to control both the location and timing of new microtubule growth. The conserved core of the nucleating machinery is the γ-tubulin small complex (γTuSC), a 300 kDa V-shaped structure with two copies of γ-tubulin and one each of the accessory proteins GCP2 and GCP3, which are distant homologs of each other. GCP2 and GCP3 form the elongated arms of the complex, with γ-tubulin at each tip of the V[1,2]. Low-resolution structural studies of isolated γTuSCs showed that it is flexible, with a hinge-like motion near the center of the GCP3 arm[2]. In most eukaryotes several other accessory proteins, GCP4-6, assemble with multiple γTuSCs to form the γ-tubulin ring complex (γTuRC)[3,4]. γTuRC has long been thought to function as a template, presenting a ring of γ-tubulins from which microtubules grow[3–7].

Saccharomyces cerevisiae lacks the γTuRC-specific accessory proteins found in other eukaryotes, and nucleates microtubules from γTuSC oligomers. These oligomers are anchored to the nuclear face of the spindle pole body by the coiled-coil protein Spc110[8,9]. Isolated γTuSCs have a weak propensity to self-assemble, and the N-terminal domain of Spc110 ($Spc110^{1–220}$) stabilizes these interactions to promote formation of extended spiral-shaped oligomers that have 13 γ-tubulins per turn[10], matching the protofilament number of *in vivo* microtubules[11]. Extended γTuSC polymers are not observed at spindle pole bodies[12], and although some estimates of the subunit number have been made[13], the overall size and organization of the functional γTuSC oligomer *in vivo* is unclear.

While the nucleation activity of yeast γTuSC is entirely dependent on its oligomerization, unexpectedly the oligomers are configured with microtubule-like γ-tubulin lateral contacts only between γTuSCs, while within each γTuSC the two γ-tubulins are held apart in an open conformation[2,10]. A consequence of the staggered lateral γ-tubulin interactions is a γTuSC ring with a pitch ~25 Å larger than that of microtubules (Supplementary Fig. 1). This conformation seems inconsistent with γTuSC assemblies acting as efficient microtubule templates; indeed, MT nucleation experiments showed only a modest enhancement over background. Based on flexibility observed within individual γTuSCs[2], however, we proposed that an allosterically regulated conformational change could result in a precise match to microtubule geometry, forming a template with increased nucleating activity[5,10].

Here, we set out to determine the structure of the functional state of γTuSC rings. We demonstrate that *in vivo* the minus ends of microtubules are anchored to the spindle pole body via a γTuSC ring that is in a closed conformation and has a defined number of subunits. While the *in vivo* drivers of ring closure are unknown, we could trap a closed state of γTuSC oligomers by disulfide crosslinking, and determined its structure at 6.9 Å resolution by cryo-EM. The closed state closely resembles the structure observed at minus ends, and conformational changes within each γTuSC result in a nearly perfect match between the γ-tubulin ring and thirteen protofilament microtubule geometries. The closed state is more active than the open state, confirming that γTuRC activity can be conformationally regulated. We also show that yeast γTuSC is much more active with yeast tubulin than with vertebrate tubulin, demonstrating the importance of species specificity in

nucleating activity. The high-resolution structure of the closed state allowed us to generate a pseudo-atomic model that provides a more detailed view of the interactions of components within the γTuSC and the nature of assembly contacts between γTuSCs.

RESULTS

γTuSC binds microtubules in a closed conformation

A key question is whether or not γTuSCs can actually form a structure that better matches microtubule symmetry. To answer this, we determined the conformational state of γTuSC rings interacting with microtubules at the spindle pole. We examined the *in situ* structure of microtubule minus ends attached to the nuclear face of purified spindle pole bodies using cryo-electron tomography (Fig. 1a). We averaged 1156 individual capped microtubule minus ends to generate a structure at 38 Å resolution (0.5 Fourier Shell Correlation (FSC) cutoff criterion). The structure reveals an asymmetric cap in which individual γTuSC subunits can be discerned in most directions. The γTuSCs form a lock-washer shaped spiral that rises 120 Å (Fig. 1b, Supplemental Movie 1), similar to the pitch of 13-protofilament microtubules[14]. This pitch is in contrast to the 147 Å pitch of reconstituted γTuSC–Spc110$^{1–f220}$ spirals[10], indicating that when bound to microtubules *in vivo* the conformation of the γTuSC ring is different than that observed for our unbound rings *in vitro*[2,10].

Spc110 promotes formation of a defined yeast γTuRC

The structure of capped minus ends also reveals the number of γTuSC oligomers *in vivo*. It has been assumed that functional γTuSC oligomers would have either six copies (with twelve γ-tubulins and a gap at the thirteenth position), seven copies (with an overlapping, inaccessible fourteenth γ-tubulin at the end), or be variable in number[6,15,16]. In the minus end structure the last γTuSC can be see to overlap vertically with the first γTuSC (Figure 1b), indicating that the ring is formed from seven subunits. Unlike these defined seven subunit rings, *in vitro* assembly of γTuSC and Spc110$^{1–220}$ yields extended spirals[10]. However, we found that a longer Spc110 fragment (residues 1–401), with an additional 180 residues of predicted coiled coil, limited γTuSC assemblies to single rings and smaller oligomers, suggesting Spc110 sterically interferes with addition of more than seven γTuSCs (Fig. 1c,d). Thus, Spc110 both promotes γTuSC assembly and limits oligomer size, forming well-defined yeast γTuRCs.

γTuSC oligomers trapped in a closed state

Since γTuSCs adopts a closed, microtubule-like geometry when interacting with microtubules, we sought to trap this closed state with engineered disulfide bonds to test the functional consequences of closure. Assuming that in a closed state γ-tubulin makes lateral contacts between the M– and H1–S2 loops similar to those observed in the microtubule lattice[14] or γ-tubulin crystals[17,18] (Fig. 2a), we designed four sets of paired cysteine mutations: Asn57 Gly288, Ser58 Gly288, Asp128 Ser291, and Arg161 Arg341. We predicted the sites to be juxtaposed at the inter-γTuSC assembly interface, but widely separated at the intra γTuSC interface (Fig. 2a). Thus, under oxidizing conditions a disulfide bond should readily form between γ-tubulins from adjacent γTuSCs, but would only form between γ-tubulins within the same γTuSC if that γTuSC sampled a closed state. Disulfide

bond formation was only observed in the N57C G288C and S58 G288C mutants. Of the two S58C G288C was better behaved in terms of oligomeric assembly, so we pursued structural and functional characterization of this complex, which we refer to as γTuSC^{CC}. The γTuSC^{CC} mutations were introduced into yeast on the only copy of γ-tubulin, where they did not affect viability or metaphase spindle organization (Supplementary Fig. 2). Thus, the mutations do not impair γTuSC function in the context of the cell.

Under reducing conditions individual γTuSC^{CC} had the same overall structure as the wildtype complex[2] (Supplementary Fig. 3a). Wildtype γTuSC has a weak propensity to self-assemble into ring-like oligomers under a narrow range of salt concentrations (<200 mM KCl) and pH (6.4–7.0). After removal of reducing reagents, however, γTuSC^{CC} spontaneously assembled into large oligomers at pH 7.6 and 500 mM KCl, conditions that strongly disfavor spontaneous assembly of wildtype γTuSC (Supplementary Fig. 3b). This suggested that inter-γTuSC disulfide bonds stabilize weak interactions between γTuSCs. SDS-PAGE of non-reduced γTuSC^{CC} revealed a ladder of cross-linked γ-tubulin oligomers, indicating that disulfide crosslinks had formed both within and between γTuSCs (Supplementary Fig. 3c). The presence of γ-tubulin oligomers with greater than two chains means that both inter- and intra-γTuSC disulfide crosslinks were formed, indicating trapping of a novel conformation of γTuSC that allowed formation of intra-γTuSC disulfide.

Next, we co-purified the γTuSC^{CC}–Spc110$^{1–220}$ complex and observed that under reducing conditions it formed filaments similar to the wildtype complex. Under weakly oxidizing conditions, however, there were clearly two populations of filaments in the sample, one similar to the open wildtype filaments (Fig. 2b, blue arrows), and a new, more compact or closed form with a different helical pitch (Fig. 2b, orange arrows). The power spectrum of single filaments of the open form had a strong layer line at 147 Å, corresponding to the pitch of the wildtype filament, while the closed form had a layer line at 122 Å, very close to the pitch of a 13 protofilament microtubule. Single filaments appeared to be predominantly of one form or the other, suggesting a cooperative transition from the open to closed morphology.

The structure of closed γTuSC oligomers

We determined the structure of the closed form of γTuSC^{CC}–Spc110$^{1–220}$ filaments by cryo-EM and iterative helical real space reconstruction[19]. To minimize heterogeneity in filament morphology γTuSC^{CC}–Spc110$^{1–220}$ was extensively dialyzed against an oxidizing buffer to promote full disulfide crosslinking (Supplementary Fig. 3d,e). An initial structure was determined at 9.4 Å resolution, from about 94,400 γTuSC subunits. To eliminate residual open-closed heterogeneity in the filaments we sorted the dataset by comparing filament segments to the initial γTuSC^{CC} and the open wildtype structures, and omitted segments that matched better to the open structure (Supplementary Fig. 3f). This yielded a final dataset with about 76,000 γTuSC subunits, and a structure at 6.9 Å resolution (Supplementary Fig. 3g); the map appears to have anisotropic resolution, with the core density (N-terminal domains of GCP2 and GCP3) more well defined than peripheral densities (C-terminal domains of GCP2 and GCP3, and γ-tubulin).

The refined helical symmetry parameters for the closed structure (−55.4° rotation and 18.8 Å rise per subunit, versus −54.3° rotation 22.2 Å rise for the open structure) match 13-protofilament microtubule geometry (Fig. 3a), and are a close match to the helical pitch of the subtomogram average of capped minus ends from spindle pole bodies (Fig. 1b, Supplemental Movie 2). Moreover, in contrast to the staggered pairs of γ-tubulins in the open state, the intra- and inter-γTuSC lateral contacts are very similar to each other, and closely resemble the microtubule lattice (Fig. 3b). Thus, in a single turn of the closed state, the ring of γ-tubulins is positioned to act as a nearly perfect microtubule template.

The closed conformation enhances nucleation activity

The similarity to the microtubule lattice suggested that the nucleating activity of γTuSC would be enhanced in the closed state. We tested the difference in activity between the open and closed states with solution nucleation assays. We previously tested the nucleation activity of γTuSC in the context of filaments formed in the presence of $Spc110^{1–220}$ [10]. This likely underestimated the full activity because only γTuSCs at the end of a filament would have been accessible for interaction with α/β-tubulin. Here, we used individual γTuRCs in which all of the γ-tubulin is available for interaction with α/β-tubulin, formed with the longer $Spc110^{1–401}$ construct that promotes assembly but blocks filament extension (Fig. 1d).

We compared nucleating activity of reduced and oxidized single rings of γTuSC–$Spc110^{1–401}$ and $γTuSC^{CC}$–$Spc110^{1–401}$. Assays performed with mammalian brain tubulin showed only a 2–3 fold increase in activity over buffer controls when using assembled yeast γTuSCs[10]. Given the quality of the symmetry match, we became concerned that there could be some problem in using mammalian tubulin with yeast γTuSCs. So despite general assumptions of strong conservation of tubulins across species, we repeated these assays with wild-type γTuSC and purified recombinant *S. cerevisiae* α/β-tubulin[20]. With yeast tubulin we observed an approximately 300-fold increase in the number of microtubules (Fig. 3c,d), indicating a remarkably strong species-specificity in the γTuSC:α/β-tubulin interaction (Supplementary Fig. 4a).

The activities of γTuSC and $γTuSC^{CC}$ were tested under reducing (open) and oxidizing (closed) conditions. Wild-type γTuSC had similar nucleation rates under both conditions, while $γTuSC^{CC}$ nucleation was similar to wildtype under reducing conditions but doubled under oxidizing conditions (Fig. 3c,d). Thus, artificially forcing the geometry of the γTuSC ring to better match that of the microtubule results in enhanced nucleating activity. While the improvement demonstrates the importance of geometric fidelity, the modest increase suggests that other conformational changes, such as a curved to straight transition within the γ-tubulin19, may be required to fully activate the complex.

Pseudo-atomic model of γTuSC

We generated a pseudo-atomic model of γTuSC by fitting and refining homology models of γ-tubulin, GCP2, and GCP3 into the cryo-EM density of a single closed state γTuSC subunit (Fig. 4a,b) and the lower resolution open state we determined previously[10]. We faced several challenges in generating the model: the very low sequence identity between GCP2

and GCP3 with GCP4 (the only homolog with a crystal structure determined) made generating reliable homology models difficult, GCP2 and GCP3 are in different conformations than GCP4, and the anisotropic resolution of the EM structure led to less reliable fitting of the C-terminal domains of GCP2 and GCP3 and γ-tubulin. We developed several new tools to perform the modeling and to validate the model; the approach is outlined below in Methods, and a full description of the modeling procedure will be described elsewhere.

GCP2 and GCP3, which have similar overall shapes, were distinguished by previous labeling experiments[1]. The primary difference between the open and closed states is the degree of flexing in GCP2 and GCP3. Both change conformation, with GCP3 straightening by about 9° and GCP2 bending by about 8° in the closed state (Supplementary Fig. 5a). In the closed state GCP2 and GCP3 are similar to each other and to the human GCP4 crystal structure, while GCP2 and GCP3 are in different flexed conformations in the open state (Supplementary Fig. 5b-e).

Density in the EM map that we previously suggested corresponds to part of Spc110[10] is more easily resolved in the new, higher-resolution map and now clearly resembles a two-stranded coiled coil. The model includes 44 residues of Spc110 as a generic two-stranded coiled coil (Fig. 4a). This density makes contacts with N-terminal regions of GCP2 and GCP3, with closest contacts near the base of GCP2 and the side of the coiled coil. Near the top (as depicted in Supplementary Fig. 5f), the Spc110 density splays apart, with one strand bending back toward GCP3, and the other extending away from GCP2 toward a γ-tubulin in the next layer of the helix. This model accounts for about 20% of the mass of the $Spc110^{1–220}$ construct. Much of the remainder of the molecule is likely near the center of the filament, where the ordered density on the outer surface connects to disordered density than runs through the core of the structure (Supplementary Fig. 5g). This positioning of Spc110 is consistent with the fact that longer lengths of coiled coil inhibit filament elongation (Fig. 1d), as adding additional mass to the center of the filament would likely disrupt the helical packing.

The model also provides new insights into the contacts between γ-tubulin and GCP2 and GCP3 (Fig 4b). Both GCP2 and GCP3 C-terminal domains make contacts with the minus end longitudinal surface of γ-tubulin, with the strongest contacts made with the T7 loop of γ-tubulin. The major difference between GCP2 and GCP3 in their interactions with γ-tubulin is an interaction between the H1-S2 loop of γ-tubulin with a loop in GCP3; the corresponding region of GCP2 is shifted away from γ-tubulin (Fig. 4b). The H1-S2 loop is at the lateral γ-tubulin interaction surface, and the interactions with GCP3 may serve to modulate lateral interactions.

DISCUSSION

The conformational change from the open to closed form of γTuSC is driven by flexing of GCP2 and GCP3, distant homologs of GCP4. In the open state the conformations of both GCP2 and GCP3 differ from GCP4, whereas in the closed state all three are in similar conformations (Supplementary Fig. 5a-e). This suggests that specific evolutionary changes

in GCP2 and GCP3 have stabilized their open, less active, conformations. The advantage of stabilizing the lower-activity state would be the ability to rapidly and specifically up-regulate γTuRC activity through allosteric activation.

The closed state is about twice as active as the open state, indicating that nucleating activity can be modulated by γTuSC conformation (Fig. 3). Importantly, yeast γTuRC demonstrated strong species specificity, being about 100-fold more active with yeast tubulin than with vertebrate tubulin. Previous nucleation assays, all performed with mammalian brain tubulin, found animal γTuRC to be much more active than the yeast counterpart[3,10,21,22]. However, indicate similar activity levels when the tubulin and γTuRC species are matched, emphasizing the importance of pairing tubulin and γTuRC from the same species in microtubule nucleation assays (Supplementary Fig. 4a). A number of amino acid substitutions between vertebrate and yeast sequences at the α-tubulin to γ-tubulin contact surfaces may account for the species specificity (Supplementary Fig. 4b,c).

The modest two-fold increase in activity we see on transition to the closed state is in line with enhancement levels previously observed with γTuRC activating proteins in metazoans. The addition of CDK5RAP2 activating protein to isolated human γTuRCs resulted in 5-fold enhancement of activity. Overexpression or depletion of CDK5RAP2 resulted in large-scale changes to the microtubule cytoskeleton in cells, suggesting that small shifts in the activity of the nucleating complex can have a large impact on cytoskeletal organization[22]. It is also possible that, in our artificial cross-linked system, other potentially important allosteric activations are not being recapitulated. For example, α/β-tubulin undergoes a dramatic curved-to-straight conformational change on polymerization[23,24], and a similar transition may accompany normal closure of γTuSC but not be induced in our cross-linked system, thus underestimating the enhancement of nucleation in a natively closed structure.

A single turn of the $\gamma TuSC^{CC}$ closed state provides a model for the full γTuRC (Fig. 5a). From this we extrapolated a structural model of γTuRC bound to a microtubule, assuming that longitudinal contacts between γ-tubulin and α-tubulin are similar to the α-to β-tubulin contacts (Fig. 5b, Supplemental Movie 3). This model, in both overall morphology and helical symmetry, is remarkably similar to the microtubule minus end we observed in SPBs. In the model, thirteen γ-tubulins make contact with the microtubule; a fourteenth γ-tubulin, bound to GCP2 in the terminal γTuSC, lies directly below the first γ-tubulin, but does not make contact with the microtubule. Intriguingly, a novel interaction appears between one end of the ordered Spc110 density and the H6-H7 loop of the fourteenth γ-tubulin, suggesting a possible role for Spc110 in stabilizing the γTuRC ring at this overlapping position (Fig. 5c). In addition to the 13 longitudinal contacts between γ- and α-tubulin around the ring, the model predicts a single lateral contact between α-tubulin and γ-tubulin at the first position in the ring; a lateral interaction between the GCP3 C-terminal domain and an adjacent β-tubulin may also occur here (Fig 5d).

A large number of phosphorylation sites have been identified on γ-tubulin, GCP2 and GCP3 in *S. cerevisiae*[25–30]. Phosphorylation at a few sites has been shown to affect organization of the mitotic spindle[28,30,31], but the functional roles of most sites remain unknown. Mapping the sites on the γTuRC model shows they fall broadly into three categories: on the exterior

of the γTuRC, at the exposed plus end of γ-tubulin, and on the interior of the γTuRC (Supplementary Fig. 6). Exterior sites may be involved in modulating γTuRC interaction with binding partners, potentially affecting localization or activation. Sites at the plus end of γ-tubulin would be expected to directly modulate interactions with α/β-tubulin; similarly, sites at the lateral contact surfaces between GCP3 or γ-tubulin and α/β-tubulin may directly influence microtubule interactions (Fig. 5d). The phosphorylation sites on the ring interior, lying mostly near the minus end of γ-tubulin, would likely be inaccessible to kinases when γTuRC is bound to a microtubule, suggesting that phosphorylation at these sites occurs when γTuRCs are unoccupied, or possibly prior to assembly of γTuSCs into γTuRC and may serve to down regulate nucleation activity.

The transition from an open to a closed state likely provides an allosteric mechanism for modulating γTuSC activity. It remains to be seen what factor or factors are involved in promoting this transition *in vivo*, and post-translational modification of γTuSC components[28,31] or direct binding by regulatory proteins may be required[22,32,33]. Regulation of γTuRC at the levels of γTuSC assembly, post-translational modification, and open-to-closed conformation are likely all involved in providing precise control of nucleating activity.

ONLINE METHODS

Spindle pole body purification and imaging

Spindle pole bodies from *Saccharomyces cerevisiae* were purified following previous published procedures [34,35]. The purified SPB sample, initially in high concentration of sucrose, was first dialyzed at 4°C overnight in a buffer containing 10 mM Bis-Tris/Cl (pH=6.5), 0.1 mM $MgCl_2$, 20% (v/v) DMSO. Next day, after mixing with 10 nm colloid gold, the sample was applied onto either a home-made holey carbon grid or a Quantifoil grid (PSI, Inc.) in a humidity chamber, then blotted and plunged into liquid ethane using a home-made plunger or a Vitrobot (FEI, Inc.). Frozen grids were stored in liquid nitrogen before use. Tomography data were collected on a Polara electron microscope (FEI, Inc.) running at 300kV. A post-column energy filter (GIF, Gatan, Inc.) was used and the slit width was set at 25 eV. Automatic data collection was carried out by UCSF Tomography software [36]. Single-axis tilt series were collected at a nominal magnification of 41,000. Images of dimension 2032x2032 were recorded on a CCD camera (UltraCam, Gatan, Inc.). The final pixel size on the images was 5.32 Å. The specimen was tilted from −60° to +60° in 1.5° step. The microscope defocus values were set in the range of 10 to 15 μm. The accumulated dose for each tilt series was ~60 $e^{-}/Å^2$.

Subvolume averaging of capped minus ends

For averaging γ-TuRC, the minus-end caps of microtubules attached to the nuclear face of the spindle pole body were identified manually. A total of 1156 subtomograms containing the MT minus-end were selected from 61 tomograms. They were boxed out and subjected to reference-free alignment by either a maximum-likelihood algorithm in Xmipp package [37] or a constrained cross correlation algorithm [38]. The alignment was carried out progressively with improvement in resolution. The structure converged after about 5 rounds of iterations

Generation of γTuSC^{CC} and Spc110$^{1–401}$ expression vectors

Spc110$^{1–401}$ was generated using Spc110 and GST DNA from the Spc110-GST pFastBac vector[21]. Primers were designed to amplify the Spc110$^{(1–401)}$ coding sequence while adding: 1) a BamHI site immediately upstream of the open reading frame; 2) a PstI site immediately downstream of the 401st Spc110 codon. Primers were designed to amplify the GST coding sequence while adding: 1) a PstI site followed by a TEV cleavage site immediately upstream of the GST open reading frame; 2) a HindIII site immediately downstream of the GST stop codon. The resulting PCR products were cloned into the Invitrogen Zero Blunt TOPO vector according to the manufacturer's instructions. BamHI and PstI were used to excise Spc110$^{(1–401)}$ and HindIII and PstI were used to excise TEV-GST from their respective TOPO vectors. The resulting fragments were ligated into pFastBac (Invitrogen) linearized using HindIII and BamHI. The Bac-to-Bac baculovirus expression system (Invitrogen) was used to produce protein from Sf9 cells according to the manufacturer's instructions using Sf-900 II SFM liquid media (Invitrogen) supplemented with 2.5% fetal bovine serum.

To generate γTuSC^{CC}, S58 and G288 of γ-tubulin were mutated to cysteines using the QuikChange Multi Site-Directed Mutagenesis Kit (Agilent Technologies) according to the manufacturer's instructions. The resulting mutant sequence was PCR amplified and cloned into the Invitrogen Zero Blunt TOPO vector according to the manufacturer's instructions. XhoI and HindIII were used to excise the mutant Tub4 sequence. The resulting fragment was ligated into pFastBac (Invitrogen) linearized with the same enzymes.

For viability testing, integrating vectors based on the pRS306[39] backbone were constructed. These contained either wild-type or mutant (S58C G288C) Tub4. 432 bp of upstream and 334 bp of downstream flanking genomic DNA sequence was included in the vector surrounding the Tub4 coding sequence.

Preparation of recombinant γTuSC and γTuSC complexes

γTuSC or γTuSC^{CC} was co-expressed with GST-tagged Spc110 constructs in Sf9 cells and purified as described[10]. Briefly, cell lysate was incubated with glutathione resin, washed in H100 (40 mM Hepes PH 7.6, 100 mM KCl, 1 mM EGTA, 1mM $MgCl_2$), and eluted from the resin by cleavage of the GST tag with TEV protease as the final purification step. For cryo-EM γTuSC^{CC}-Spc110$^{1–220}$ filaments were at 2 mg/ml total protein in H100 and 1 mM oxidized gluathione. Negative stain samples were prepared as described[40] in 0.75% uranyl formate, and cryo-EM samples were prepared on C-FLAT holey carbon grids[41] using a Vitrobot (FEI Co.).

Imaging and three-dimensional reconstruction of γTuSC and γTuSC complexes

Negative stain samples were imaged on a Tecnai Spirit G^2 Biotwin electron microscope (FEI, Inc.) operating at 120 kV, and images were recorded on an Ultrascan 4000 CCD detector (Gatan, Inc.). Cryo-EM images were recorded on a Tecnai TF20 electron microscope operating at 200 kV, and images were recorded on 8k×8k TemCam-F816 camera (TVIPS, GmbH) with a pixel size of 0.94 Å/pixel. Images were acquired in a defocus range of 0.8–2 μm. Defocus was determined with CTFFIND[42], and each micrograph was corrected by application of a Wiener filter. Particles were boxed out in 485

Å segments, overlapping by 448 Å. After several initial rounds of unrestrained alignment search the particles were centred with respect to the helix axis by integer pixel shifts.

Iterative helical real space reconstruction was performed essentially as described by Egelman[43] and Sasche, et al.[44], using SPIDER[45], using a low-pass filtered cylinder was used as the initial reference volume. Initial helical symmetry parameters were taken from the open state γTuSC filament (−54.3° rotation, 22.2 Å rise per subunit), and refined at each iteration with the program hsearch_lorentz[43]. Initial centering of the particles was carried out on 4x binned images, with subsequent refinement on 2x binned images. An initial structure was determined at ~9.6 Å resolution. To reduce open to closed heterogeneity in the data set cross correlations were calculated for each helical segment to the initial reconstruction and the original open state structure[10], and particles matching better to the open state were omitted from further rounds of refinement. After sorting five rounds of unrestrained alignment search were carried out with the 2x binned images. To minimize effects of bending in the helix each segment was masked to 200 Å along the helical axis and 340 Å perpendicular to the axis with a cosine-edged mask. These masked particles were then subjected to five rounds of local refinement of the unbinned images. Resolution was assessed by the $FSC_{0.5}$ criterion. Volumes were viewed and segmented using Chimera[46].

Fluorescence imaging of yeast cells carrying the γTuSC^{CC} mutation

All yeast strains were derived from W303. Fluorescent tags were introduced by PCR as described (http://depts.washington.edu/yeastrc “Plasmids and Protocols”), and *TUB4(S58C/G288C)* was integrated at the *TUB4* locus into *glr1*Δ cells, which carry a deletion for the gene encoding glutathione reductase and have high levels of oxidized glutathione[47]. The *glr1*Δ strain was used to increase the favorability of forming disulfides in the *TUB4* mutant. Live cells were mounted for microscopy on a 1% agarose pad[48]. Images were acquired at a single focal plane, with 1x1 binning, using a U Plan Apo 100× objective lens (1.35 NA), an Olympus IX70 inverted microscope, and a CoolSnap HQ digital camera (Photometrics) managed by softWorX software (Applied Precision). Exposures were 0.4 s for both mCherry and GFP. The images were processed as previously described[49] using custom Matlab programs (available upon request) to identify and quantify mCherry and GFP fluorescence intensities.

Yeast strains used

All yeast strains also have *ade2-1oc ade3*Δ*-100 can1-100 his3-11,15 leu2-3,112 trp1-1 ura3-1* except as shown. Yeast strains used: **KFY36-13C** *MATalpha LEU2::GFP-TUB1 lys2*Δ*::HIS3 SPC42-mCherry::hphMX;* **KFY42-1C** *MAT**a** LEU2::GFP-TUB1 lys2*Δ*::HIS3 glr1*Δ*::TRP1 SPC42-mCherry::hphMX;* **KFY91** *MAT**a** LEU2::GFP-TUB1 lys2*Δ*::HIS3 glr1*Δ*::TRP1 SPC42-mCherry::hphMX TUB4(S58C/G288C);* **KFY135-8B** *MAT**a** lys2*Δ*::HIS3 TUB4(S58C/G288C)::URA3::tub4*Δ*::kanMX glr1*Δ*::TRP1 SPC42-mCherry::hphMX NUF2-GFP::kanMX;* **KFY135-47A** *MAT**a** glr1*Δ*::TRP1 SPC42-mCherry::hphMX NUF2-GFP::kanMX;* **KFY138-5A** *MAT**a** NUF2-GFP::kanMX SPC42-mCherry::hphMX*

Microtubule nucleation assays

Yeast tubulin was over-expressed and purified as described[20]. Pure γTuSC-Spc110, γTuSC alone, or buffer control (40mM K-HEPES pH6.9, 100mM KCl, 1mM EGTA, 1mM $MgCl_2$, 20% glycerol, 100 μM GTP, 100 μM oxidized or reduced glutathione) and *S. cerevisiae* tubulin were diluted at the appropriate concentrations into microtubule assembly buffer (80mM K-PIPES pH 6.9, 125mM KCl, 20% glycerol, 1mM EGTA, 1mM $MgCl_2$, 1mM GTP, 100 μM oxidized or reduced glutathione) on ice. Reactions were incubated at 30°C for 20 min, fixed 3 min in 10 volumes of 1% glutaraldehyde in BRB80 (80mM K-PIPES pH 6.9,1mM EGTA, 1mM $MgCl_2$), and then diluted 10 times into BRB80 (final volume 1.5ml). 1ml of the resulting fixed reactions was layered onto 20% glycerol/BRB80 cushions and centrifuged for 45 min, 24,000×g, onto 18mm round coverslips. Microtubules were visualized on the coverslips by immunofluorescence with FITC-mouse-anti-μ-tubulin (Sigma F2168) and 5–10 fields of microtubules were counted for each experiment.

Homology modeling and flexible fitting

Models of γ-TuSC were computed using a combination of comparative protein structure modeling and flexible fitting into the EM density map of the closed state. To create a template structure for γ-TuSC, we rigidly docked 2 copies of the crystal structure of human GCP4 into the density map using UCSF Chimera[46]. Independently, initial alignment of the sequences in the TUBGCP family was performed with Promals3D[50]. Next, we produced an initial homology model of the GCP2–GCP3 dimer based on the initial alignment and the GCP4 template, using MODELLER 9.13[51]. The alignment was then iteratively refined by hand to improve the fit of the model into the density map. Using the final alignment, 200 homology models of the dimer were produced. We completed each dimer into a model of γ-TuSC by rigidly docking two copies of γ-tubulin and a coiled-coil fragment of Spc110. An additional neighboring copy of the complete γ-TuSC structure was added to model the inter-γ-TuSC interface. Subsequently, each γ-TuSC dimer was flexibly fitted into the density map using MDFF[52], with additional restraints to preserve helical symmetry, secondary structure, and conformation of the γ-tubulin domains. The best scoring model, as defined by the highest cross-correlation coefficient between the model and the map, was subjected to additional local sampling to estimate model precision, using MODELLER to randomize loops and MDFF to re-optimize the structures. The above process was repeated for the open state, using the open-state EM density map and the final alignment from the modeling of the closed state.

Supplementary Material

Refer to Web version on PubMed Central for supplementary material.

ACKNOWLEDGEMENTS

The authors are grateful to Michael Braunfeld and Xueming Li for assistance with cryo-EM data collection, and Luke Rice for help with over-expression and purification of yeast tubulin. This work was funded by the Howard Hughes Medical Institute and National Institutes of Health grants R01 GM031627 to D.A.A., R01 GM040506 to T.N.D., and T32 GM007270 to K.K.F.

REFERENCES

1. Choy RM, Kollman JM, Zelter A, Davis TN, Agard DA. Localization and orientation of the gamma-tubulin small complex components using protein tags as labels for single particle EM. J Struct Biol. 2009; 168:571–574. [PubMed: 19723581]
2. Kollman JM, et al. The structure of the gamma-tubulin small complex: implications of its architecture and flexibility for microtubule nucleation. Mol Biol Cell. 2008; 19:207–215. [PubMed: 17978090]
3. Oegema K, et al. Characterization of two related Drosophila gamma-tubulin complexes that differ in their ability to nucleate microtubules. J Cell Biol. 1999; 144:721–733. [PubMed: 10037793]
4. Zheng Y, Wong ML, Alberts B, Mitchison T. Nucleation of microtubule assembly by a gamma-tubulin-containing ring complex. Nature. 1995; 378:578–583. [PubMed: 8524390]
5. Kollman JM, Merdes A, Mourey L, Agard DA. Microtubule nucleation by gamma-tubulin complexes. Nat Rev Mol Cell Biol. 2011; 12:709–721. [PubMed: 21993292]
6. Moritz M, Braunfeld MB, Guenebaut V, Heuser J, Agard DA. Structure of the gamma-tubulin ring complex: a template for microtubule nucleation. Nat Cell Biol. 2000; 2:365–370. [PubMed: 10854328]
7. Oakley BR, Oakley CE, Yoon Y, Jung MK. Gamma-tubulin is a component of the spindle pole body that is essential for microtubule function in Aspergillus nidulans. Cell. 1990; 61:1289–1301. [PubMed: 2194669]
8. Kilmartin JV, Goh PY. Spc110p: assembly properties and role in the connection of nuclear microtubules to the yeast spindle pole body. EMBO J. 1996; 15:4592–4602. [PubMed: 8887551]
9. Sundberg HA, Davis TN. A mutational analysis identifies three functional regions of the spindle pole component Spc110p in Saccharomyces cerevisiae. Mol Biol Cell. 1997; 8:2575–2590. [PubMed: 9398677]
10. Kollman JM, Polka JK, Zelter A, Davis TN, Agard DA. Microtubule nucleating gamma-TuSC assembles structures with 13-fold microtubule-like symmetry. Nature. 2010; 466:879–882. [PubMed: 20631709]
11. Tilney LG, et al. Microtubules: evidence for 13 protofilaments. J Cell Biol. 1973; 59:267–275. [PubMed: 4805001]
12. O'Toole ET, Winey M, McIntosh JR. High-voltage electron tomography of spindle pole bodies and early mitotic spindles in the yeast Saccharomyces cerevisiae. Mol Biol Cell. 1999; 10:2017–2031. [PubMed: 10359612]
13. Erlemann S, et al. An extended gamma-tubulin ring functions as a stable platform in microtubule nucleation. J Cell Biol. 2012; 197:59–74. [PubMed: 22472440]
14. Sui H, Downing KH. Structural basis of interprotofilament interaction and lateral deformation of microtubules. Structure. 2010; 18:1022–1031. [PubMed: 20696402]
15. Keating TJ, Borisy GG. Immunostructural evidence for the template mechanism of microtubule nucleation. Nat Cell Biol. 2000; 2:352–357. [PubMed: 10854326]
16. Wiese C, Zheng Y. A new function for the gamma-tubulin ring complex as a microtubule minus-end cap. Nat Cell Biol. 2000; 2:358–364. [PubMed: 10854327]
17. Aldaz H, Rice LM, Stearns T, Agard DA. Insights into microtubule nucleation from the crystal structure of human gamma-tubulin. Nature. 2005; 435:523–527. [PubMed: 15917813]
18. Rice LM, Montabana EA, Agard DA. The lattice as allosteric effector: structural studies of alphabeta- and gamma-tubulin clarify the role of GTP in microtubule assembly. Proc Natl Acad Sci U S A. 2008; 105:5378–5383. [PubMed: 18388201]
19. Egelman EH. The iterative helical real space reconstruction method: surmounting the problems posed by real polymers. J Struct Biol. 2007; 157:83–94. [PubMed: 16919474]
20. Johnson V, Ayaz P, Huddleston P, Rice LM. Design, overexpression, and purification of polymerization-blocked yeast alphabeta-tubulin mutants. Biochemistry. 2011; 50:8636–8644. [PubMed: 21888381]
21. Vinh DB, Kern JW, Hancock WO, Howard J, Davis TN. Reconstitution and characterization of budding yeast gamma-tubulin complex. Mol Biol Cell. 2002; 13:1144–1157. [PubMed: 11950928]

22. Choi YK, Liu P, Sze SK, Dai C, Qi RZ. CDK5RAP2 stimulates microtubule nucleation by the gamma-tubulin ring complex. J Cell Biol. 2010; 191:1089–1095. [PubMed: 21135143]
23. Lowe J, Li H, Downing KH, Nogales E. Refined structure of alpha beta-tubulin at 3.5 A resolution. J Mol Biol. 2001; 313:1045–1057. [PubMed: 11700061]
24. Ravelli RB, et al. Insight into tubulin regulation from a complex with colchicine and a stathmin-like domain. Nature. 2004; 428:198–202. [PubMed: 15014504]
25. Holt LJ, et al. Global analysis of Cdk1 substrate phosphorylation sites provides insights into evolution. Science. 2009; 325:1682–1686. [PubMed: 19779198]
26. Albuquerque CP, et al. A multidimensional chromatography technology for in-depth phosphoproteome analysis. Mol Cell Proteomics. 2008; 7:1389–1396. [PubMed: 18407956]
27. Holinger EP, et al. Budding yeast centrosome duplication requires stabilization of Spc29 via Mps1-mediated phosphorylation. J Biol Chem. 2009; 284:12949–12955. [PubMed: 19269975]
28. Keck JM, et al. A cell cycle phosphoproteome of the yeast centrosome. Science. 2011; 332:1557–1561. [PubMed: 21700874]
29. Lin TC, et al. Phosphorylation of the yeast gamma-tubulin Tub4 regulates microtubule function. PLoS One. 2011; 6:e19700. [PubMed: 21573187]
30. Vogel J, et al. Phosphorylation of gamma-tubulin regulates microtubule organization in budding yeast. Dev Cell. 2001; 1:621–631. [PubMed: 11709183]
31. Nazarova E, et al. Distinct roles for antiparallel microtubule pairing and overlap during early spindle assembly. Mol Biol Cell. 2013; 24:3238–3250. [PubMed: 23966467]
32. Samejima I, Miller VJ, Groocock LM, Sawin KE. Two distinct regions of Mto1 are required for normal microtubule nucleation and efficient association with the gamma-tubulin complex in vivo. J Cell Sci. 2008; 121:3971–3980. [PubMed: 19001497]
33. Goshima G, Mayer M, Zhang N, Stuurman N, Vale RD. Augmin: a protein complex required for centrosome-independent microtubule generation within the spindle. J Cell Biol. 2008; 181:421–429. [PubMed: 18443220]

REFERENCES FOR ONLINE METHODS

34. Rout MP, Kilmartin JV. Yeast spindle pole body components. Cold Spring Harbor symposia on quantitative biology. 1991; 56:687–692. [PubMed: 1819516]
35. Donaldson AD, Kilmartin JV. Spc42p: a phosphorylated component of the S. cerevisiae spindle pole body (SPD) with an essential function during SPB duplication. Journal of cell biology. 1996; 132:887–901. [PubMed: 8603920]
36. Zheng QS, Braunfeld MB, Sedat JW, Agard DA. An improved strategy for automated electron microscopic tomography. Journal of structural biology. 2004; 147:91–101. [PubMed: 15193638]
37. Scheres SHW, Melero R, Valle M, Carazo J-M. Averaging of electron subtomograms and random conical tilt reconstructions through likelihood optimization. Structure (London, England 1993). 2009; 17:1563–1572.
38. Förster F, Pruggnaller S, Seybert A, Frangakis AS. Classification of cryo-electron sub-tomograms using constrained correlation. Journal of structural biology. 2008; 161:276–286. [PubMed: 17720536]
39. Sikorski RS, Hieter P. A system of shuttle vectors and yeast host strains designed for efficient manipulation of DNA in Saccharomyces cerevisiae. Genetics. 1989; 122:19–27. [PubMed: 2659436]
40. Ohi M, Li Y, Cheng Y, Walz T. Negative Staining and Image Classification - Powerful Tools in Modern Electron Microscopy. Biol Proced Online. 2004; 6:23–34. [PubMed: 15103397]
41. Quispe J, et al. An improved holey carbon film for cryo-electron microscopy. Microsc Microanal. 2007; 13:365–371. [PubMed: 17900388]
42. Mindell JA, Grigorieff N. Accurate determination of local defocus and specimen tilt in electron microscopy. J Struct Biol. 2003; 142:334–347. [PubMed: 12781660]
43. Egelman EH. A robust algorithm for the reconstruction of helical filaments using single-particle methods. Ultramicroscopy. 2000; 85:225–234. [PubMed: 11125866]

44. Sachse C, et al. High-resolution electron microscopy of helical specimens: a fresh look at tobacco mosaic virus. J Mol Biol. 2007; 371:812–835. [PubMed: 17585939]

45. Frank, J. Three-Dimensional Electron Microscopy of Macromolecular Assemblies. Academic Press, Inc.; San Diego: 1996.

46. Pettersen EF, et al. UCSF Chimera--a visualization system for exploratory research and analysis. J Comput Chem. 2004; 25:1605–1612. [PubMed: 15264254]

47. Muller EG. A glutathione reductase mutant of yeast accumulates high levels of oxidized glutathione and requires thioredoxin for growth. Mol Biol Cell. 1996; 7:1805–1813. [PubMed: 8930901]

48. Muller EG, et al. The organization of the core proteins of the yeast spindle pole body. Mol Biol Cell. 2005; 16:3341–3352. [PubMed: 15872084]

49. Shimogawa MM, Widlund PO, Riffle M, Ess M, Davis TN. Bir1 is required for the tension checkpoint. Mol Biol Cell. 2009; 20:915–923. [PubMed: 19056681]

50. Pei J, Kim BH, Grishin NV. PROMALS3D: a tool for multiple protein sequence and structure alignments. Nucleic Acids Res. 2008; 36:2295–2300. [PubMed: 18287115]

51. Sali A, Blundell TL. Comparative protein modelling by satisfaction of spatial restraints. J Mol Biol. 1993; 234:779–815. [PubMed: 8254673]

52. Trabuco LG, Villa E, Mitra K, Frank J, Schulten K. Flexible fitting of atomic structures into electron microscopy maps using molecular dynamics. Structure. 2008; 16:673–683. [PubMed: 18462672]

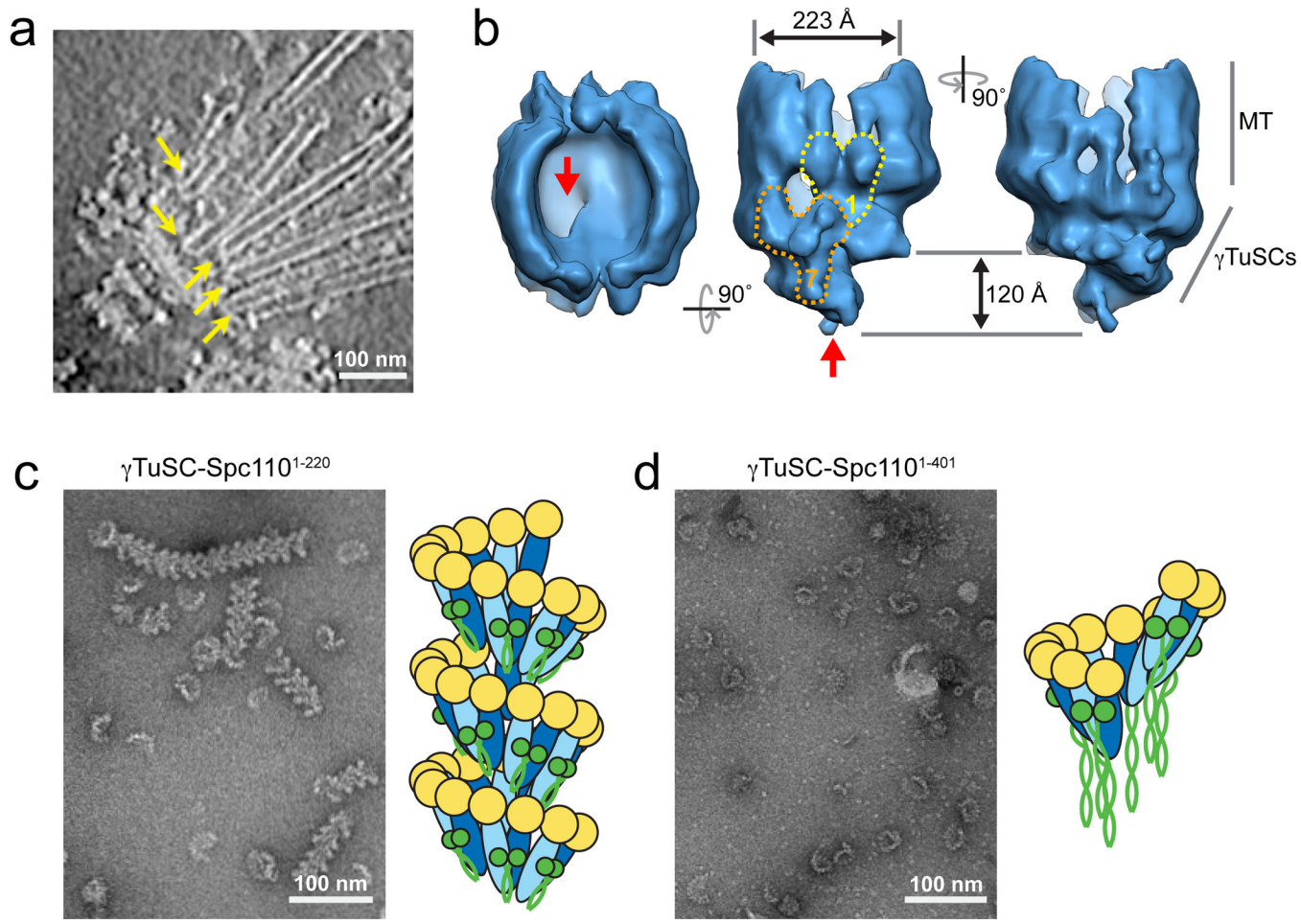

Figure 1. The yeast γTuRC is formed from seven γTuSCs and is limited in size by Spc110

a) A slice from a tomogram of isolated spindle pole bodies clearly shows the capped minus ends of microtubules. b) Subtomogram averaged structure of microtubule minus end. Red arrows indicate the position of the half-subunit overlap between the first and seventh γTuSC (outlined in yellow and orange, respectively). The 120 Å longitudinal rise of the γTuSC ring is indicated. c) γTuSC assembles extended filaments when bound to Spc110$^{1–220}$. Spc110 binds the outer surface of γTuSC, and fits within the groove of the filament (cartoon). d) Spc110$^{1–401}$ promotes assembly of γTuSC rings, but prevents extension beyond a single ring, suggesting that the longer predicted coiled-coil domain interferes with formation of oligomers greater than 7 γTuSC subunits.

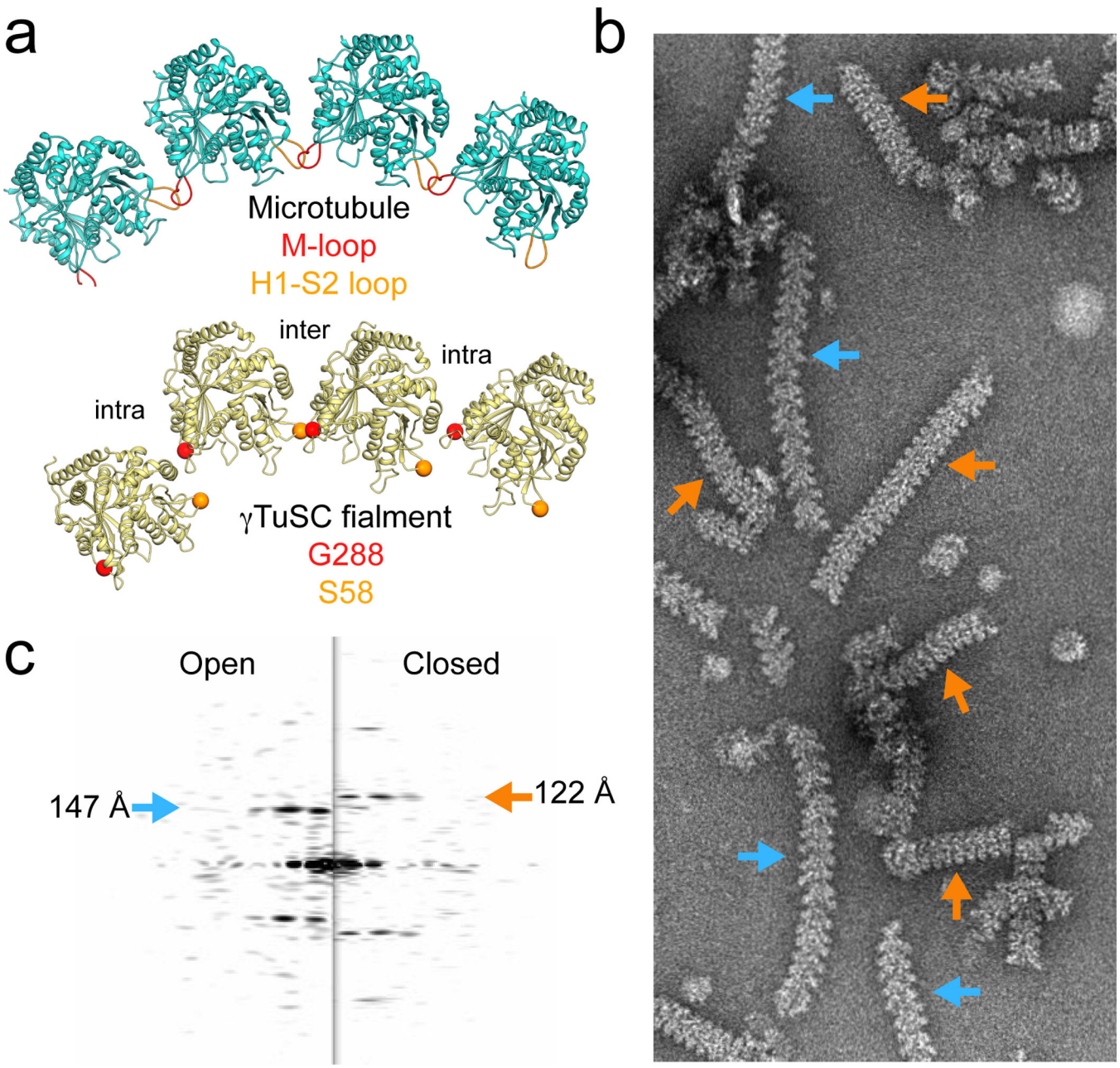

Figure 2. Engineered disulfides alter γTuSC filament morphology

a) The lateral interface between β-tubulin subunits in the 13-protofilament microtubule, and the corresponding lateral interactions between γ-tubulins in the open state filament are shown. b) Negative stain electron micrograph of the double mutant S58C G288C ($\gamma TuSC^{CC}$) in complex with $Spc110^{1–220}$ show two distinct filament morphologies were apparent (blue and orange arrows). c) Power spectra of individual filaments of different morphologies from (b) have different layer line spacing indicating different helical pitch.

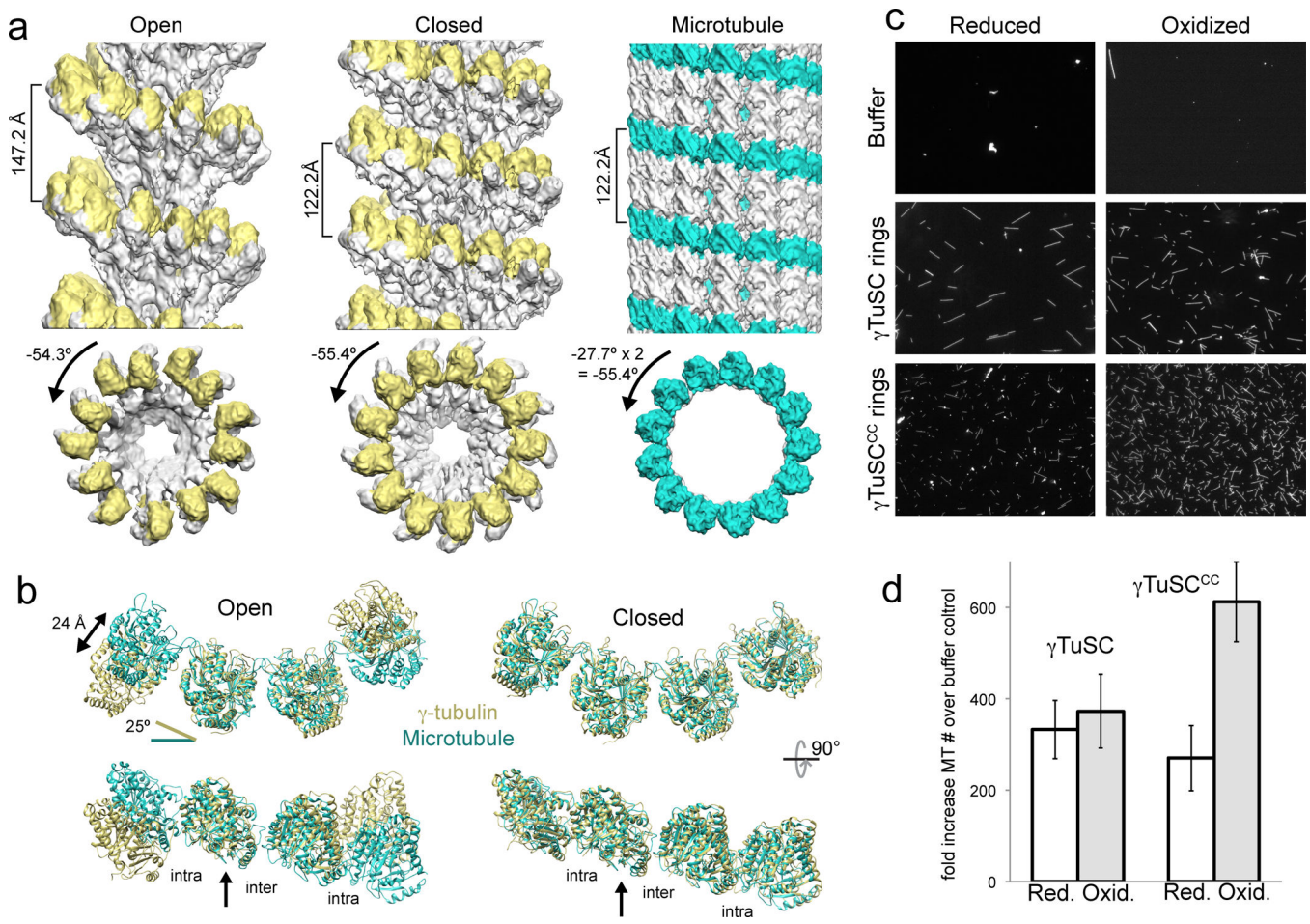

Figure 3. In the closed state γTuSC matches microtubule symmetry and has increased nucleation activity

a) The open state γTuSC filament, closed state γTuSC^{cc} filament, and 13-protofilament microtubule structure. γ-tubulin is highlighted in gold in the γTuSC structures, and the pitch of the 3-start helix in the microtubule is highlighted in cyan. Refined helical pitch and rotation per subunit are indicated. b) Superposition of the open and closed γ-tubulin rings (gold) on the microtubule (cyan). The γ-tubulin indicated by the arrow was superimposed on a β-tubulin from the microtubule. c) Representative fluorescence images of solution microtubule nucleation experiments d) Microtubules were counted for five fields per experiment, and the fold increase over buffer/γTuSC alone controls is plotted for reduced (Red.) and oxidized (Oxid.) states (n=4 independent experiments; error bars represent the s.e.m.). Activity of γTuSCs alone was similar to buffer controls, with only a few microtubules on the entire coverslip (not shown). T-tests confirm significant differences between activity of γTuSC110^{CC} complexes under oxidizing and reducing conditions ($p \leq 0.013$), or between mutant and wild-type: ($p \leq 0.055$).

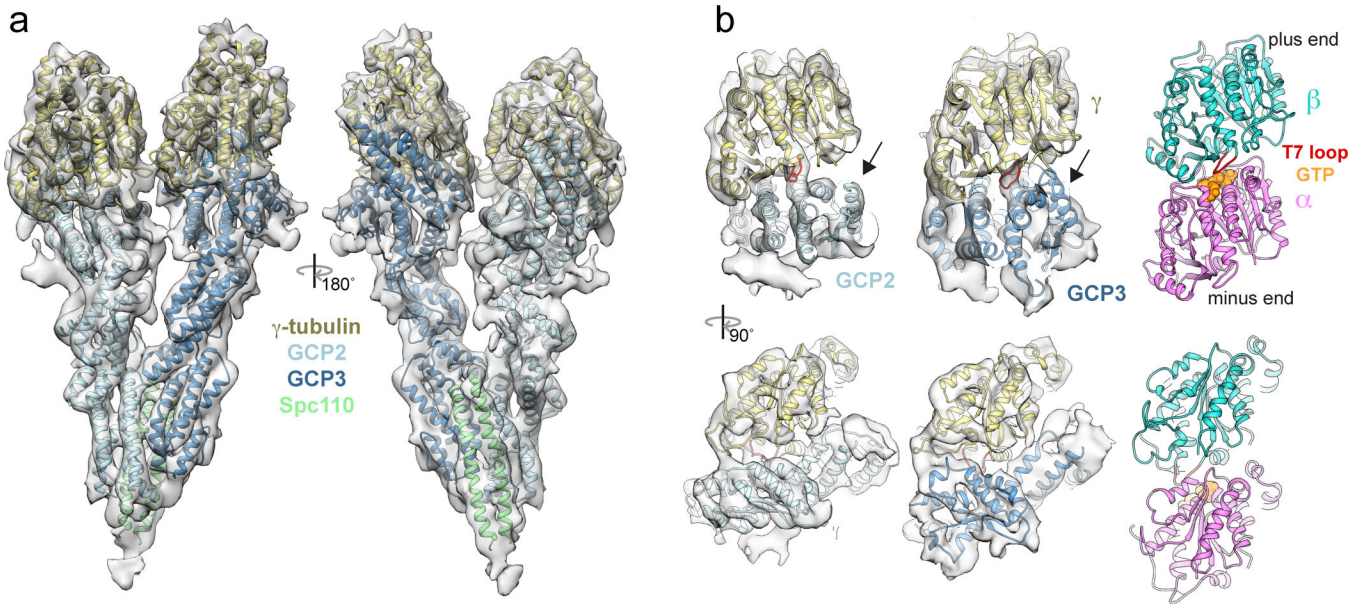

Figure 4. Pseudo-atomic model of γTuSC in the closed conformation

a) The pseduo-atomic model of γTuSC (ribbon diagram) fit into the cryo-EM structure (semi-transparent surface). b) Close up views of the interactions of γ-tubulin with the C-terminal domains of GCP2 and GCP3, compared to longitudinal interactions within the α/β-tubulin heterodimer, with the T7 loop highlighted in red. The top view is the view from inside the microtubule, and the bottom view is looking at lateral interaction surfaces. Contacts are made between the H1–S2 loop of γ-tubulin and residues 524–536 of GCP3; the corresponding region of GCP2 is shifted away from γ-tubulin in the GCP2 structure (arrows).

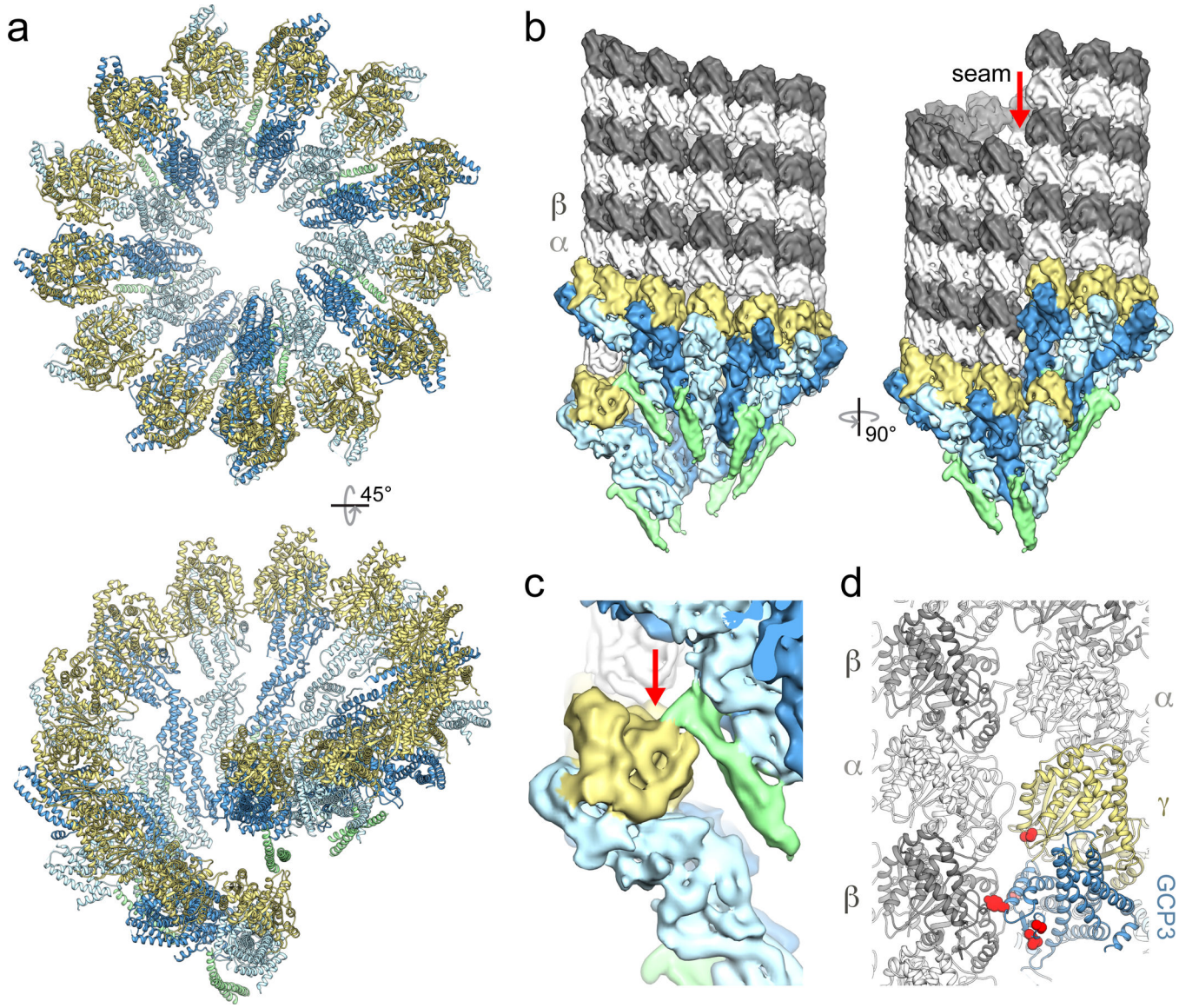

Figure 5. Pseudo-atomic model of γTuRC and its interactions with microtubules

a) The pseudo-atomic model of a complete yeast γTuRC with seven γTuSCs. b) A model of yeast γTuRC interacting with the minus end of a microtubule. c) A potential contact between the last γ-tubulin in the ring, which is not directly interacting with the microtubule, and Spc110 bound to the first γTuSC (arrow) is seen in the $\gamma TuSC^{CC}$ structure. d) Magnified view of interactions between the first γTuSC and the microtubule. Known phosphorylation sites on γTuSC that could potentially modulate lateral interactions with α/β-tubulin are indicated with red spheres.